6-D Movable Antenna for Fairness-Aware Integrated Sensing and Communication Systems

Wenjun Zhang, Qiong Wu, *Senior Member, IEEE*, Pingyi Fan, *Senior Member, IEEE*, Kezhi Wang, *Senior Member, IEEE*, Guoqiang Mao, *Fellow, IEEE*, and Khaled B. Letaief, *Fellow, IEEE*

***Abstract*— Six-dimensional movable antenna (6DMA) is a promising solution to improve the performance of future wireless networks by flexibly adjusting three-dimensional (3D) positions and rotations of antenna surfaces. Previous studies have verified the potential of 6DMA in communication/sensing, failing to explore its integration into integrated sensing and communication (ISAC) systems. In this letter, we propose a fairness-aware 6DMA-enabled ISAC system for non-uniform user distribution. Specifically, we introduce a functionally reconfigurable 6DMA-based base station (BS) architecture, in which the mode selection, 3D positions, and rotations of all 6DMA surfaces, as well as the receive beamforming matrices at the BS are jointly optimized under a max–min fairness principle to prioritize the performance of the most vulnerable user. We aim to maximize the minimum signal-to-interference-plus-noise ratio (SINR) across all ISAC users. To tackle the non-convex optimization problem, we propose an alternating optimization (AO) framework that decomposes the non-convex optimization problem into three subproblems and alternately solves them in an iterative manner. Finally, simulation results demonstrate the superiority of the proposed scheme, which achieved the improvement of system performance while ensuring the fairness of communication and sensing.**

***Index Terms*— 6DMA, ISAC, position and rotation optimization, max–min fairness, alternating optimization.**

Received 31 December 2025; revised 26 February 2026; accepted 31 March 2026. Date of publication 6 April 2026; date of current version 10 April 2026. This work was supported in part by Jiangxi Province Science and Technology Development Program under Grant 20242BCC32016, in part by the National Natural Science Foundation of China under Grant 61701197, in part by the Basic Research Program of Jiangsu under Grant BK20252084, in part by the National Key Research and Development Program of China under Grant 2021YFA1000500(4), in part by the Research Grants Council under the Areas of Excellence Scheme under Grant AoE/E-601/22-R, and in part by the 111 Project under Grant B23008. The associate editor coordinating the review of this article and approving it for publication was X. Shao. *(Corresponding author: Qiong Wu.)*

Wenjun Zhang and Qiong Wu are with the School of Internet of Things Engineering, Jiangnan University, Wuxi 214122, China, and also with the School of Information Engineering, Jiangxi Provincial Key Laboratory of Advanced Signal Processing and Intelligent Communications, Nanchang University, Nanchang 330031, China (e-mail: wenjunzhang@stu.jiangnan.edu.cn; qiongwu@jiangnan.edu.cn).

Pingyi Fan is with the Department of Electronic Engineering, State Key Laboratory of Space Network and Communications, Beijing National Research Center for Information Science and Technology, Tsinghua University, Beijing 100084, China (e-mail: fpy@tsinghua.edu.cn).

Kezhi Wang is with the Department of Computer Science, Brunel University of London, UB8 3PH Middlesex, U.K. (e-mail: Kezhi.Wang@brunel.ac.uk).

Guoqiang Mao is with the School of Transportation, Southeast University, Nanjing 211189, China (e-mail: g.mao@ieee.org).

Khaled B. Letaief is with the Department of Electrical and Computer Engineering, The Hong Kong University of Science and Technology, Hong Kong (e-mail: eekhaled@ust.hk).

Digital Object Identifier 10.1109/LWC.2026.3681324

I. Introduction

INTEGRATED sensing and communication (ISAC) is an essential technology for the sixth-generation (6G) wireless network. It shares hardware, spectrum, and even signal waveforms, significantly improving spectral efficiency, energy utilization, and hardware cost [1]. However, ISAC systems find it difficult to ensure both reliable communication and precise localization simultaneously in the case of the non-uniform distribution of heterogeneous users, which poses a challenge to the flexibility and adaptability of antenna systems.

Traditional fixed-position antenna (FPA) arrays suffer from rigid physical configurations, making them inadequate to address the non-uniform user distribution. This limitation results in constrained beamforming gain and difficult interference management, thereby restricting the performance of ISAC systems. In response to the challenge, six-dimensional movable antenna (6DMA) has emerged. The positions and rotations of 6DMA surfaces can be flexibly adjusted, enabling the reconfiguration of beam steering, coverage patterns, and gain distribution for electromagnetic waves [2].

The potential of 6DMA in communication [3], [4], [5], [6], [7], [8] and sensing [8], [9] has been demonstrated. By jointly optimizing the three-dimensional (3D) positions and rotations of 6DMA surfaces, 6DMA can effectively improve the wireless network capacity [3], [4]. Some studies have investigated the integration of 6DMA with beamforming [5], multiple input multiple output (MIMO) [6], and intelligent reflecting surfaces (IRS) [7]. 6DMA can also be used for improving wireless sensing accuracy by lowering the Cramér–Rao bound (CRB) for direction-of-arrival (DoA) estimation [9]. Hierarchically Tunable 6DMA was further proposed for communication/sensing [8]. However, existing works regard communication and sensing as isolated tasks, and there are no related studies on 6DMA-enabled ISAC yet. Motivated by this, we propose a fairness-aware 6DMA-enabled ISAC system.

More specifically, we introduce a functionally reconfigurable 6DMA-BS architecture that jointly optimizes the mode selection, 3D positions, and rotations of all 6DMA surfaces, as well as the receive beamforming matrices at the base station (BS) to maximize the minimum signal-to-interference-plus-noise ratio (SINR) among all ISAC users. An alternating optimization (AO) algorithm is proposed to address this non-convex optimization problem. Simulation results verify the superiority of the proposed scheme.[1]

[1]The source code is available at: https://github.com/qiongwu86/6D-Movable-Antenna-for-Fairness-aware-Integrated-Sensing-and-Communication-System

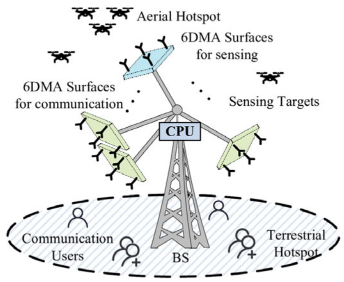

Fig. 1. System architecture of the 6DMA-BS-enabled ISAC network.

II. System Model and Problem Formulation

As illustrated in Fig. 1, we consider a 6DMA-BS serving b terrestrial communication users, indexed by the set $\mathcal{B} = \{1, \cdots, B\}$, and sensing L hovering autonomous aerial vehicles (AAVs), indexed by the set $\mathcal{L} = \{1, \cdots, L\}$. Communication users and AAV positions exhibit non-uniform spatial distributions due to the existence of hotspots. The 6DMA-BS comprises Q independently configurable 6DMA surfaces, denoted by the set $\mathcal{Q} = \{1, \cdots, Q\}$. Each surface is a uniform planar array (UPA) of a given size, consisting of $M \geq 1$ antennas, denoted by the set $\mathcal{M} = \{1, \cdots, M\}$. All surfaces are connected to a central processing unit (CPU) via flexible cables embedded in extendable and rotatable rods, allowing the CPU to adjust the 3D positions and rotations of the surfaces. The CPU can switch the mode of each surface by introducing a binary variable $\rho_q \in \{0, 1\}$, $\forall q \in \mathcal{Q}$, where $\rho_q = 1$ if the q-th 6DMA surface is configured in communication mode to serve communication users, and $\rho_q = 0$ indicates it is configured in sensing mode for AAV localization. The mode is reconfigured via software-defined radio (SDR).

A. 6DMA-BS Model

With the 6DMA-BS's reference position serving as the origin, a global Cartesian coordinate system (CCS) o-xyz is established. The pose of the q-th 6DMA surface is parameterized by six degrees of freedom, i.e., $\mathbf{p}_q = [x_q, y_q, z_q]^T \in \mathcal{V}$ for the 3D positions and $\mathbf{r}_q = [\alpha_q, \beta_q, \gamma_q]^T$ for the 3D rotations. Here, $\mathcal{V}$ represents a given 3D space where the 6DMA surface can be freely positioned and rotated. The coordinates x_q, y_q, and z_q denote the center of the q-th 6DMA surface in o-xyz, while its rotation angles relative to the x-, y-, and z-axes are denoted by α_q, β_q, and $\gamma_q \in [0, 2\pi)$, respectively. Given $\mathbf{r}_q$, the corresponding rotation matrix can be defined as

$$\mathbf{V}(\mathbf{r}_q) = \begin{bmatrix} c_{\beta_q} c_{\gamma_q} & c_{\beta_q} s_{\gamma_q} & -s_{\beta_q} \\ s_{\beta_q} s_{\alpha_q} c_{\gamma_q} - c_{\alpha_q} s_{\gamma_q} & s_{\beta_q} s_{\alpha_q} s_{\gamma_q} + c_{\alpha_q} c_{\gamma_q} & c_{\beta_q} s_{\alpha_q} \\ c_{\alpha_q} s_{\beta_q} c_{\gamma_q} + s_{\alpha_q} s_{\gamma_q} & c_{\alpha_q} s_{\beta_q} s_{\gamma_q} - s_{\alpha_q} c_{\gamma_q} & c_{\alpha_q} c_{\beta_q} \end{bmatrix}. \tag{1}$$

Here, $c_a = \cos(a)$ and $s_a = \sin(a)$. Next, a local CCS o'-$x'y'z'$ is established for each 6DMA surface, with its origin at the surface's center and the x-axis oriented along the normal direction of the surface. In the local CCS of the 6DMA surface, the m-th antenna's position is $\tilde{\mathbf{u}}_m$, which can be transformed into the global CCS as

$$\mathbf{u}_{q,m}(\mathbf{p}_q, \mathbf{r}_q) = \mathbf{p}_q + \mathbf{V}(\mathbf{r}_q)\tilde{\mathbf{u}}_m, \quad m \in \mathcal{M}, q \in \mathcal{Q}, \tag{2}$$

According to [3], the following practical constraints need be considered when rotating/positioning 6DMA surfaces:

$$\mathbf{n}(\mathbf{r}_q)^T(\mathbf{p}_j - \mathbf{p}_q) \leq 0, \quad \forall q, j \in \mathcal{Q}, j \neq q, \tag{3}$$

$$\mathbf{n}(\mathbf{r}_q)^T \mathbf{p}_q \geq 0, \quad \forall q \in \mathcal{Q}, \tag{4}$$

$$\|\mathbf{p}_q - \mathbf{p}_j\|_2 \geq d_{\min}, \quad \forall q, j \in \mathcal{Q}, j \neq q. \tag{5}$$

where the transformation $\mathbf{n}(\mathbf{r}_q) = \mathbf{R}(\mathbf{r}_q)\tilde{\mathbf{n}}$ converts the local CCS normal vector $\tilde{\mathbf{n}}$ to the global CCS for the q-th 6DMA surface. Constraint (3) avoids inter-surface signal reflections, while constraint (4) prevents CPU-induced signal obstruction. Furthermore, constraint (5) ensures that the distance between the centers of any pair of 6DMA surfaces must be at least $d_{\min}$ to avoid surface overlap and coupling effects.

The pointing vector $\mathbf{f}$, determined by the azimuth angle $\phi \in [-\pi, \pi]$ and elevation angle $\theta \in [-\pi/2, \pi/2]$ of the signal arriving at the BS, can be expressed as $\mathbf{f} = [\cos(\theta)\cos(\phi), \ \cos(\theta)\sin(\phi), \ \sin(\theta)]^T$. Thus, the steering phase of the m-th antenna on the q-th 6DMA surface is denoted by $\psi_{q,m} = -\frac{2\pi}{\lambda}\mathbf{f}^T\mathbf{u}_{q,m}(\mathbf{p}_q, \mathbf{r}_q)$, where λ is the carrier wavelength. Taking o as the reference point, the steering vector of q-th surface is

$$\mathbf{a}(\mathbf{p}_q, \mathbf{r}_q) = \left[e^{j\psi_{q,1}}, e^{j\psi_{q,2}}, \cdots, e^{j\psi_{q,M}}\right]^T \in \mathbb{C}^{M\times 1}. \tag{6}$$

We assume all antennas share the same radiation pattern, but their effective gains differ due to varying rotations, i. e.,

$$g(\mathbf{r}_q) = 10^{A(\tilde{\phi}_q, \tilde{\theta}_q)/10}, \tag{7}$$

where $\tilde{\phi}_q = \mathrm{atan2}(\tilde{y}_q, \tilde{x}_q)$ and $\tilde{\theta}_q = \arcsin(\tilde{z}_q)$ are azimuth and elevation angles in the local CCS of the q-th 6DMA surface with $[\tilde{x}_q, \tilde{y}_q, \tilde{z}_q]^T = -\mathbf{V}(\mathbf{r}_q)^{-1}\mathbf{f} = -\mathbf{V}(\mathbf{r}_q)^T\mathbf{f}$. The effective antenna gain $A(\tilde{\phi}_q, \tilde{\theta}_q)$ in dBi is modeled as

$$A(\tilde{\phi}_q, \tilde{\theta}_q) = G_{\max} - \min\left\{-\left[A_H(\tilde{\phi}_q) + A_V(\tilde{\theta}_q)\right], G_s\right\}, \tag{8}$$

where $G_{\max}$ denotes the maximum directional gain of each antenna element in the main lobe direction. The horizontal radiation pattern $A_H(\tilde{\phi}_q)$ and vertical radiation pattern $A_V(\tilde{\theta}_q)$ are respectively given by $A_H(\tilde{\phi}_q) = -\min\left\{12\left(\frac{\tilde{\phi}_q}{\phi_{3\mathrm{dB}}}\right)^2, G_s\right\}$, $A_V(\tilde{\theta}_q) = -\min\left\{12\left(\frac{\tilde{\theta}_q}{\theta_{3\mathrm{dB}}}\right)^2, G_v\right\}$. Here, $\phi_{3\mathrm{dB}}$ and $\theta_{3\mathrm{dB}}$ refer to the 3-dB beamwidth, while G_s and G_v specify front-to-back ratio and sidelobe level limit.

B. Communication Model

In the uplink scenario where B single-antenna terrestrial users communicate with the 6DMA-BS, the effective line-of-sight (LoS) communication channel between user b and the BS can be modeled as

$$\mathbf{h}_{c,b}(\mathbf{p}, \mathbf{r}, \boldsymbol{\rho}) = \sqrt{\nu_b}e^{-j\frac{2\pi d_b}{\lambda}}\left[\rho_1\sqrt{g(\mathbf{r}_1)}\mathbf{a}(\mathbf{p}_1, \mathbf{r}_1)^T, \cdots, \rho_Q\sqrt{g(\mathbf{r}_Q)}\mathbf{a}(\mathbf{p}_Q, \mathbf{r}_Q)^T\right]^T \in \mathbb{C}^{MQ\times 1}. \tag{9}$$

Here, $\mathbf{p} = \left[\mathbf{p}_1^T, \cdots, \mathbf{p}_Q^T\right]^T$, $\mathbf{r} = \left[\mathbf{r}_1^T, \cdots, \mathbf{r}_Q^T\right]^T$, and $\boldsymbol{\rho} = [\rho_1, \cdots, \rho_Q]^T$. The path gain is defined as $\nu_b = \zeta_0 d_b^{-\kappa}$, where κ is the path loss exponent, ζ_0 indicates the reference channel power at distance d_0, while $d_b \geq d_0$ represents the distance between user b and the 6DMA-BS's reference position.

The BS utilizes a linear receive beamforming vector $\mathbf{w}_{c,b} \in \mathbb{C}^{MQ\times 1}$ to decode the transmitted signal x_b from user b, i.e.,

$$y_{c,b} = \mathbf{w}_{c,b}^H \mathbf{h}_{c,b}(\mathbf{p}, \mathbf{r}, \boldsymbol{\rho}) x_b + \mathbf{w}_{c,b}^H \sum_{j=1, j\neq b}^{B} \mathbf{h}_{c,j}(\mathbf{p}, \mathbf{r}, \boldsymbol{\rho}) x_j + \mathbf{w}_{c,b}^H \mathbf{n}, \tag{10}$$

where $x_b \sim \mathcal{N}_c(0, P_{c,b})$ represents the transmission symbol of user b with transmit power $P_{c,b}$, and $\mathbf{n} \sim \mathcal{CN}\left(0, \sigma^2 \mathbf{I}_{MQ}\right)$ denotes the additive white Gaussian noise (AWGN) vector at the BS, with σ^2 being the noise power. The SINR for decoding the information from user b is then given by

$$\gamma_{c,b} = \frac{P_{c,b} \left| \mathbf{w}_{c,b}^H \mathbf{h}_{c,b}(\mathbf{p}, \mathbf{r}, \boldsymbol{\rho}) \right|^2}{\sum_{j=1, j\neq b}^{B} P_{c,j} \left| \mathbf{w}_{c,b}^H \mathbf{h}_{c,j}(\mathbf{p}, \mathbf{r}, \boldsymbol{\rho}) \right|^2 + \sigma^2 \|\mathbf{w}_{c,b}\|^2}. \tag{11}$$

C. Sensing Model

The round-trip sensing channel vector from the BS to AAV l and back to the BS can be expressed as

$$\mathbf{h}_{s,l}(\mathbf{p}, \mathbf{r}, \boldsymbol{\rho}) = \alpha_l \sqrt{\nu_l} e^{-j\frac{4\pi d_l}{\lambda}} \left[(1-\rho_1) g(\mathbf{r}_1) \mathbf{a}(\mathbf{p}_1, \mathbf{r}_1)^T, \cdots, (1-\rho_Q) g(\mathbf{r}_Q) \mathbf{a}(\mathbf{p}_Q, \mathbf{r}_Q)^T \right]^T \in \mathbb{C}^{MQ\times 1}, \tag{12}$$

where the path gain is modeled as $\nu_l = \zeta_0^2 d_l^{-2\kappa}$, α_l is the target reflection coefficient related to the AAV's RCS, and d_l represents the distance between the 6DMA-BS and AAV l. To simultaneously detect all AAVs, the BS transmits the sensing signal vector $\mathbf{s} = [s_1, \cdots, s_L]^T$, where s_l is the dedicated probing signal for AAV l, satisfying $\mathbb{E}\left[|s_l|^2\right] = P_{s,l}$ with $P_{s,l}$ denoting the probing power allocated to AAV l. The echo signal from AAV l, demodulated via the receive beamforming vector $\mathbf{w}_{s,l}$, is given by

$$y_{s,l} = \mathbf{w}_{s,l}^H \mathbf{h}_{s,l}(\mathbf{p}, \mathbf{r}, \boldsymbol{\rho}) s_l + \mathbf{w}_{s,l}^H \sum_{j=1, j\neq l}^{L} \mathbf{h}_{s,j}(\mathbf{p}, \mathbf{r}, \boldsymbol{\rho}) s_j + \mathbf{w}_{s,l}^H \mathbf{n}. \tag{13}$$

Consequently, the SINR for sensing AAV l is derived as

$$\gamma_{s,l} = \frac{P_{s,l} \left| \mathbf{w}_{s,l}^H \mathbf{h}_{s,l}(\mathbf{p}, \mathbf{r}, \boldsymbol{\rho}) \right|^2}{\sum_{j=1, j\neq l}^{L} P_{s,j} \left| \mathbf{w}_{s,l}^H \mathbf{h}_{s,j}(\mathbf{p}, \mathbf{r}, \boldsymbol{\rho}) \right|^2 + \sigma^2 \|\mathbf{w}_{s,l}\|^2}. \tag{14}$$

Given that the accurate detection probability $\propto \gamma_{s,l}$ and CRB $\propto 1/\gamma_{s,l}$, $\gamma_{s,l}$ serves as an effective metric for sensing performance.

D. Problem Formulation

To ensure fairness in both communication and sensing performance, our optimization objective maximizes the minimum SINR among all ISAC users through jointly optimizing the positions, rotations, mode of all 6DMA surfaces and the receive beamforming matrices at the BS. Accordingly, the optimization problem is formulated as

$$\text{(P1)} \quad \max_{\mathbf{p}, \mathbf{r}, \boldsymbol{\rho}, \mathbf{W}_c, \mathbf{W}_s} \quad \min \gamma_i \tag{15a}$$

$$\text{s.t.} \quad \rho_q \in \{0, 1\}, \quad \forall q \in \mathcal{Q}, \tag{15b}$$

$$\mathbf{p}_q \in \mathcal{V}, \quad \forall q \in \mathcal{Q}, \tag{15c}$$

$$\mathbf{n}(\mathbf{r}_q)^T (\mathbf{p}_j - \mathbf{p}_q) \leq 0, \quad \forall q, j \in \mathcal{Q}, j \neq q, \tag{15d}$$

$$\mathbf{n}(\mathbf{r}_q)^T \mathbf{p}_q \geq 0, \quad \forall q \in \mathcal{Q}, \tag{15e}$$

$$\|\mathbf{p}_q - \mathbf{p}_j\|_2 \geq d_{\min}, \quad \forall q, j \in \mathcal{Q}, j \neq q, \tag{15f}$$

where $\gamma_i = \gamma_{c,b}$ if $i \in \mathcal{B}$ and $\gamma_i = \gamma_{s,l}$ if $i \in \mathcal{L}$. $\mathbf{W}_c = [\mathbf{w}_{c,1}, \cdots, \mathbf{w}_{c,B}] \in \mathbb{C}^{MQ\times B}$ and $\mathbf{W}_s = [\mathbf{w}_{s,1}, \cdots, \mathbf{w}_{s,L}] \in \mathbb{C}^{MQ\times L}$ denote the receive beamforming matrices for communication and sensing, respectively. Let $\mathcal{V}$ in constraint (15b) to be a finite-sized convex space. Problem (P1) is a mixed-integer nonlinear programming (MINLP) problem due to the binary variable $\boldsymbol{\rho}$ as well as the non-convex SINR expressions and constraints (15d),(15e),(15f). The optimization problem is further challenged by the coupling of variables $\mathbf{p}$, $\mathbf{r}$ and $\boldsymbol{\rho}$ in the objective function.

III. Proposed Solution

This section presents an AO framework to address the optimization problem (P1). Firstly, the communication and sensing receive beamforming matrices are designed with fixed $\mathbf{p}$, $\mathbf{r}$ and $\boldsymbol{\rho}$. Secondly, the binary variable $\boldsymbol{\rho}$ is relaxed to continuous values, and a successive convex approximation (SCA) approach is employed to optimize it. Finally, the positions $\mathbf{p}$ and rotations $\mathbf{r}$ of all 6DMA surfaces are updated sequentially via accelerated projected gradient descent (APGD).

A. Receive Beamforming Design

With perfect channel state information (CSI) available at the BS, we apply the minimum mean square error (MMSE) method to design the receive beamforming at the BS for any given $\mathbf{p}$, $\mathbf{r}$ and $\boldsymbol{\rho}$ of 6DMA surfaces. Specifically:

$$\mathbf{W}_{c,\text{MMSE}} = \left(\mathbf{H}_c \mathbf{P}_c \mathbf{H}_c^H + \sigma^2 \mathbf{I}_{MQ} \right)^{-1} \mathbf{H}_c, \tag{16}$$

$$\mathbf{W}_{s,\text{MMSE}} = \left(\mathbf{H}_s \mathbf{P}_s \mathbf{H}_s^H + \sigma^2 \mathbf{I}_{MQ} \right)^{-1} \mathbf{H}_s, \tag{17}$$

where $\mathbf{H}_c \triangleq [\mathbf{h}_{c,1}(\mathbf{p}, \mathbf{r}, \boldsymbol{\rho}), \cdots, \mathbf{h}_{c,B}(\mathbf{p}, \mathbf{r}, \boldsymbol{\rho})]$ denotes the effective channel matrix between the BS and b communication users, and $\mathbf{P}_c \triangleq \operatorname{diag}(P_{c,1}, \cdots, P_{c,B})$ is the diagonal transmit power matrix of b communication users. Similarly, $\mathbf{H}_s$ and $\mathbf{P}_s$ represent the corresponding effective channel and diagonal probing power matrices for L AAVs, respectively.

B. Mode Selection Optimization

Given $\mathbf{p}$ and $\mathbf{r}$, the communication channel between user b and the BS $\mathbf{h}_{c,b}(\boldsymbol{\rho})$ is a linear function of $\boldsymbol{\rho}$, while the sensing channel between AAV l and the BS $\mathbf{h}_{s,l}(\boldsymbol{\rho})$ is affine w.r.t. $\boldsymbol{\rho}$. For any receive beamforming vector $\mathbf{w}_i$, the SINR numerator can be defined as $f_i(\boldsymbol{\rho}) = P_i \left| \mathbf{w}_i^H \mathbf{h}_i(\boldsymbol{\rho}) \right|^2$. Similarly, the SINR denominator can be written as $g_i(\boldsymbol{\rho}) = \sum_{j\neq i} P_j \left| \mathbf{w}_i^H \mathbf{h}_j(\boldsymbol{\rho}) \right|^2 + \sigma^2 \|\mathbf{w}_i\|^2$. To sum up, $f_i(\boldsymbol{\rho})$ and $g_i(\boldsymbol{\rho})$ are quadratic convex functions, and $\gamma_i(\boldsymbol{\rho}) = \frac{f_i(\boldsymbol{\rho})}{g_i(\boldsymbol{\rho})}$ is a non-convex fractional function.

The binary variable ρ_q is relaxed to $\tilde{\rho}_q \in [0, 1]$, and the auxiliary variable τ is introduced as the lower bound of all SINR. The resulted problem for optimizing $\boldsymbol{\rho}$ is then obtained from (P1) as

$$\text{(P2)} \max_{\tilde{\boldsymbol{\rho}}, \tau} \quad \tau \tag{18a}$$

$$\text{s.t.} \quad \gamma_i(\tilde{\boldsymbol{\rho}}) \geq \tau, \quad \forall i, \tag{18b}$$

$$0 \leq \tilde{\rho}_q \leq 1, \quad \forall q \in \mathcal{Q}, \tag{18c}$$

To address this, we introduce $\phi_i(\tilde{\boldsymbol{\rho}}, \tau) \triangleq f_i(\tilde{\boldsymbol{\rho}}) - \tau g_i(\tilde{\boldsymbol{\rho}})$, which is a difference-of-convex (DC) function w.r.t. $(\tilde{\boldsymbol{\rho}}, \tau)$. For $\phi_i(\tilde{\boldsymbol{\rho}}, \tau) \geq 0$, a conservative convex lower bound is constructed using a first-order Taylor expansion at the point $\phi_i(\tilde{\boldsymbol{\rho}}^{(t-1)}, \tau^{(t-1)})$ as

$$\phi_i(\tilde{\rho}, \tau) \geq a_i^{(t-1)} + \mathbf{b}_i^{(t-1)T}\tilde{\boldsymbol{\rho}} - c_i^{(t-1)}\tau, \tag{19}$$

where $a_i^{(t-1)} = f_i^{(t-1)} - \nabla f_i^{(t-1)T}\tilde{\boldsymbol{\rho}}^{(t-1)} + \tau^{(t-1)}\nabla g_i^{(t-1)T}\tilde{\boldsymbol{\rho}}^{(t-1)}$, $\mathbf{b}_i^{(t-1)} = \nabla_{\tilde{\boldsymbol{\rho}}} f_i(\boldsymbol{\rho}^{(t-1)}) - \tau^{(t-1)}\nabla_{\tilde{\boldsymbol{\rho}}} g_i^{(t-1)}$, $c_i^{(t-1)} = g_i^{(t-1)}$. This leads to the convex linear constraint as follows

$$a_i^{(t-1)} + \mathbf{b}_i^{(t-1)T}\tilde{\boldsymbol{\rho}} - c_i^{(t-1)}\tau \geq 0, \quad \forall i, \tag{20}$$

The resulted problem for optimizing $\tilde{\boldsymbol{\rho}}$ is from (P2) as

$$\text{(P2-a)} \max_{\tilde{\boldsymbol{\rho}}, \tau} \quad \tau \tag{21a}$$
$$\text{s.t.} \quad (20), (18c), \tag{21b}$$

This convex problem (P2-a) can be solved using linear programming methods, yielding $\tilde{\boldsymbol{\rho}} \in [0, 1]^B$. If $\tilde{\rho}_q \geq 0.5$, $\rho_q = 1$; otherwise, $\rho_q = 0$.

C. Position and Rotation Optimization

For fixed $\boldsymbol{\rho}$, $\mathbf{W}_c$, and $\mathbf{W}_c$, the optimization problem (P1) can be reformulated as

$$\text{(P3)} \max_{\mathbf{p}, \mathbf{r}} \quad \min \gamma_i \tag{22a}$$
$$\text{s.t.} \quad (15c), (15d), (15e), (15f), \tag{22b}$$

To solve this problem, we update the position and rotation of each 6DMA surface in sequence, while the positions and rotations of other surfaces remain fixed. Since $\min \gamma_i$ is non-smooth, we utilize the log-sum-exp (LSE) surrogate function for smooth approximation:

$$\tilde{f}_\mu(\mathbf{p}, \mathbf{r}) = -\frac{1}{\mu} \log \left(\sum_i \exp\left(-\mu\gamma_i(\mathbf{p}, \mathbf{r})\right) \right), \tag{23}$$

where μ is a smoothing parameter.

Given $\mathbf{r}_b$, the non-convex constraint (15f) is approximated as the following convex constraint via the first-order Taylor expansion at the value of $\mathbf{p}_q^{(t-1)}$ from the previous iteration, which is given by

$$\left(\mathbf{p}_q^{(t-1)} - \mathbf{p}_j\right)^T (\mathbf{p}_q - \mathbf{p}_j) \geq d_{\min} \left\| \mathbf{p}_q^{(t-1)} - \mathbf{p}_j \right\|_2. \tag{24}$$

Therefore, the feasible domain w.r.t. $\mathbf{p}_q$ becomes a convex set. For any subproblem $\max_{\mathbf{p}_q \in \mathcal{F}} \tilde{f}_\mu(\mathbf{p}_q)$, $\mathbf{p}_q$ is updated using APGD as follows

- Extrapolation step: $\mathbf{y} = \mathbf{p}_q + \beta_t \left(\mathbf{p}_q - \mathbf{p}_q^{(t-1)}\right)$,
- Gradient ascent step: $\mathbf{v} = \mathbf{y} + \eta \nabla \tilde{f}_\mu(\mathbf{y})$,
- Projection step: $\mathbf{p}_q = \Pi_{\mathcal{F}}(\mathbf{v})$,

where momentum coefficient $\beta_t = \frac{t-1}{t+2}$ is in the standard Nesterov form, and step size η is determined by Armijo backtracking to ensure sufficient ascent. In addition, the projection set $\mathcal{F}$ is a convex set composed of linearized constraints, defined as $\mathcal{F} = \left\{\mathbf{p}_q \in \mathbb{R}^3 | (15c), (15d), (15e), (24)\right\}$. $\Pi_{\mathcal{F}}(\cdot)$ is the Euclidean projection on the convex set $\mathcal{F}$ and can be achieved by solving the following small-scale quadratic programming (QP) problem, i.e., $\Pi_{\mathcal{F}}(\mathbf{v}) = \arg\min_{\mathbf{p}_q} \frac{1}{2}\|\mathbf{p}_q - \mathbf{v}\|^2, \quad \text{s.t.} \quad (15c), (15d), (15e), (24)$.

Algorithm 1 Proposed AO Algorithm for Solving (P1)

Input: Initial positions $\mathbf{p}^{(0)}$, rotations $\mathbf{r}^{(0)}$, mode $\boldsymbol{\rho}^{(0)}$ and the iteration numbers T_1, T_2.
for $t = 1$ **to** T_1 **do**
  Update $\mathbf{W}_c^{(t)}$ via (16), and update $\mathbf{W}_s^{(t)}$ via (17).
  for $i = 1$ **to** T_2 **do**
    Construct linearized DC constraint via (20);
    Obtain $\tilde{\boldsymbol{\rho}}^{(i)}$ by solving (P2-a);
    Update $\boldsymbol{\rho}^{(i)}$ via $\boldsymbol{\rho}^{(i)} = \text{round}\left(\tilde{\boldsymbol{\rho}}^{(i)}\right)$.
    for $q = 1$ **to** Q **do**
      Compute gradient $\nabla \tilde{f}_\mu(\mathbf{y}^{i-1})$ via (25);
      Update $\mathbf{p}_q^i$ by solving the QP problem.
  end for
  for $q = 1$ **to** Q **do**
      Compute gradient $\nabla \tilde{f}_\mu(\mathbf{y}^{i-1})$ via (25);
      Update $\mathbf{r}_q^i$ by solving the QP problem.
    end for
  end for
end for
Update $\mathbf{W}_c^{(t)}$ via (16), and update $\mathbf{W}_s^{(t)}$ via (17).
return $\mathbf{p}$, $\mathbf{r}$, $\boldsymbol{\rho}$, $\mathbf{W_c}$, and $\mathbf{W_s}$.

From the chain rule, we can obtain

$$\nabla \tilde{f}_\mu(\mathbf{y}) = \sum_i w_i(\mathbf{y}) \nabla \gamma_i(\mathbf{y}), w_i(\mathbf{y}) = \frac{e^{-\mu\gamma_i(\mathbf{y})}}{\sum_{j \neq i} e^{-\mu\gamma_j(\mathbf{y})}} \tag{25}$$

Here, $[\nabla \gamma_i(\mathbf{y})]_n = \lim_{\varepsilon \to 0} \frac{\gamma_i(\mathbf{y}+\varepsilon\mathbf{e}_n) - \gamma_i(\mathbf{y})}{\varepsilon}, n = 1, 2, 3$, with $\mathbf{e}_n$ being a vector with a one in the n-th element and zeros elsewhere.

Given $\mathbf{p}_q$, $\mathbf{r}_q$ can be optimized in the similar way. The non-convex constraints (15d) and (15e) can be converted into convex forms through a linear approximation of the rotation matrix $\mathbf{V}(\mathbf{r}_q)$, as detailed in [3]. Then, the rotation $\mathbf{r}_q$ can also be optimized using the APGD method.

The proposed AO framework for solving problem (P1) is summarized in Algorithm 1. The Algorithm 1 converges because each subproblem update guarantees a non-decreasing objective value, and all variables evolve within a compact feasible set, ensuring a monotonic and bounded objective sequence that converges to a stationary point. The overall complexity of Algorithm 1 is $\mathcal{O}\left(T_1 T_2 \left[(B+L)^2 M Q^2 + Q^3\right]\right)$.

IV. Numerical Results

In this section, we present numerical results to demonstrate the effectiveness of the proposed method. We set $\lambda = 0.125$m, $\sigma^2 = -50$dBm, $P_{c,b}{}_{b=1}^{B} = 40$mW, and $P_{s,l}{}_{l=1}^{L} = 100$mW. In addition, the total number of antennas at the 6DMA-BS is set as 64, and $\mathcal{V}$ is modeled as a cube with 1m sides. We consider three hotspots, one in the sky and two on the ground. The initial positions of all 6DMA surfaces are uniformly distributed on a sphere with radius 0.5m, generated using spherical Fibonacci lattice. The outward normal vectors of the surfaces are initialized to be radial away from the center of the sphere. The binary mode vector $\boldsymbol{\rho}$ is initialized via an alternating strategy, i.e., $\rho_q = 1$ for odd q, and $\rho_q = 0$ for even q. We consider the following schemes (with the same total number of antennas) for performance comparison: 1) Traditional FPA: Static antenna deployment; 2) Rotation-Only MA: Only the surfaces' rotations are optimized; 3) Position-Only MA: Only the surfaces' positions are

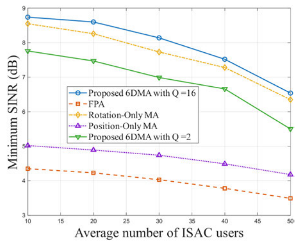

Fig. 2. Minimum SINR versus average number of ISAC users.

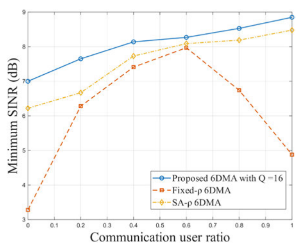

Fig. 3. Minimum SINR versus communication users radio.

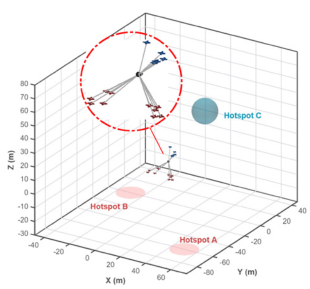

Fig. 4. Optimized positions/rotations of 6DMA surfaces for Q = 16.

optimized; 4) Fixed-$\boldsymbol{\rho}$ 6DMA: 6DMA with fixed binary mode vector $\boldsymbol{\rho}$; 5) Simulated Annealing (SA)-$\boldsymbol{\rho}$ 6DMA: 6DMA with $\boldsymbol{\rho}$ optimized via simulated annealing.

Fig. 2 shows the minimum SINR versus average number of ISAC users with a communication user ratio of 0.6. The proposed 6DMA scheme with 16 surfaces consistently achieves the highest minimum SINR across all ISCA user counts, significantly outperforming other approaches. This highlights the benefit of jointly optimizing all six degrees of freedom. Even with just two surfaces, the proposed 6DMA method still surpasses the schemes of FPA and Position-Only MA, confirming that coordinated control of positions, rotations, and mode delivers meaningful fairness improvements.

Fig. 3 presents Minimum SINR versus communication users radio with 30 ISAC users. The proposed 16-surface 6DMA scheme demonstrates consistent performance advantages across varying communication user ratios through its adaptive mode selection mechanism. The Fixed-$\boldsymbol{\rho}$ strategy fails to adjust hardware resource allocation with the increasing radio of communication users, resulting in a shortage of communication resources. The communication bottleneck leads to a significant degradation in overall performance. Although SA-$\boldsymbol{\rho}$ 6DMA scheme can perform global search, it tends to converge to suboptimal solutions in high-dimensional combinatorial spaces due to its inability to exploit structural information, resulting in inferior performance.

Fig. 4 depicts the optimized 3D positions and rotations of 16 6DMA surfaces obtained via the proposed algorithm. Owing to the spatially heterogeneous distributions of terrestrial communication users and aerial sensing targets, the surfaces naturally form two distinct functional clusters in space. Specially, one downward-pointing cluster (denoted in red for communication mode) serves communication users, while the other upward-tilted cluster (marked in blue for sensing mode) oriented toward AAVs. This spatial self-organization demonstrates the system's capability to physically reconfigure its antenna array in response to heterogeneous user distributions, while simultaneously validating the practical feasibility of the proposed optimization framework.

Additionally, the numerical results indicate that the proposed scheme typically converges within no more than 20 outer iterations ($T_1 \leq 20$) and 6 inner iterations ($T_2 \leq 6$). For a system comprising 16 surfaces and 30 ISAC users, the average computation time per inner iteration is approximately 0.42 seconds based on the current hardware condition. Given that the algorithm's runtime is significantly shorter than the reconfiguration cycle of 6DMA (which ranges from hours to even days), this computational overhead is not taken into account in the practical deployment.

V. Conclusion

The letter aims to maximize the worst SINR across all ISAC users. To this end, we developed an AO algorithm. First, the receive beamforming matrices are obtained in closed form via MMSE. Second, a SCA approach is employed to optimize the mode selection variable. Finally, we adopted a LSE approximation to circumvent the non-smoothness of the min-SINR objective, and the 3D positions and rotations of all 6DMA surfaces are updated sequentially via APGD. Numerical results demonstrated the superiority of the proposed scheme, which achieved the improvement of system performance while ensuring the fairness of communication and sensing. Future work will extend this study by considering non-ideal channel conditions and diverse radiation patterns.

References

[1] X. Shao et al., "A tutorial on six-dimensional movable antenna for 6G networks: Synergizing positionable and rotatable antennas," *IEEE Commun. Surveys Tuts.*, vol. 28, pp. 3666–3709, 2026, doi: 10.1109/COMST.2025.3602939.

[2] X. Zhu et al., "Enabling intelligent connectivity: A survey of secure ISAC in 6G networks," *IEEE Commun. Surveys Tuts.*, vol. 27, no. 2, pp. 748–781, Apr. 2025.

[3] X. Shao, Q. Jiang, and R. Zhang, "6D movable antenna based on user distribution: Modeling and optimization," *IEEE Trans. Wireless Commun.*, vol. 24, no. 1, pp. 355–370, Jan. 2025.

[4] X. Shao, R. Zhang, Q. Jiang, and R. Schober, "6D movable antenna enhanced wireless network via discrete position and rotation optimization," *IEEE J. Sel. Areas Commun.*, vol. 43, no. 3, pp. 674–687, Mar. 2025.

[5] Y. Zhang, Y. Zhang, S. Xiao, W. Tang, and Y. C. Eldar, "6D movable antenna-aided hybrid beamforming for multi-user communications," in *Proc. IEEE Globecom Workshops (GC Wkshps)*, Cape Town, South Africa, Dec. 2024, pp. 1–6.

[6] X. Shi, X. Shao, B. Zheng, and R. Zhang, "6DMA-aided cell-free massive MIMO communication," *IEEE Wireless Commun. Lett.*, vol. 14, no. 5, pp. 1361–1365, May 2025.

[7] H. Wang, X. Shao, B. Zheng, X. Shi, and R. Zhang, "Passive six-dimensional movable antenna (6DMA)-assisted multiuser communication," *IEEE Wireless Commun. Lett.*, vol. 14, no. 4, pp. 1014–1018, Apr. 2025.

[8] X. Shao, R. Zhang, and R. Schober, "Exploiting six-dimensional movable antenna for wireless sensing," *IEEE Wireless Commun. Lett.*, vol. 14, no. 2, pp. 265–269, Feb. 2025.

[9] H. Hua, Y. Zhou, W. Mei, J. Xu, and R. Zhang, "Hierarchically tunable 6DMA for wireless communication and sensing: Modeling and performance optimization," *IEEE Trans. Wireless Commun.*, vol. 25, pp. 4721–4736, 2026, doi: 10.1109/TWC.2025.3613548.